

The most massive Population III stars

Teeraparb Chantavat,¹★ Siri Chongchitnan,² and Joseph Silk^{3,4,5}

¹*Institute for Fundamental Study, Naresuan University, Phitsanulok, 65000, Thailand*

²*Warwick Mathematics Institute, University of Warwick, Zeeman Building, Coventry, CV4 7AL, United Kingdom*

³*Institut d'Astrophysique de Paris, 98 bis Boulevard Arago, 75014, Paris, France*

⁴*William H. Miller III Department of Physics and Astronomy, The Johns Hopkins University, Baltimore, MD 21218, USA*

⁵*BIPAC, Department of Physics, University of Oxford, Keble Road, Oxford OX1 3RH, UK*

Accepted XXX. Received YYY; in original form ZZZ

ABSTRACT

Recent data from the James Webb Space Telescope suggest that there are realistic prospects for detecting the earliest generation of stars at redshift ~ 20 . These metal-poor, gaseous Population III (Pop III) stars are likely in the mass range $10 - 10^3 M_{\odot}$. We develop a framework for calculating the abundances of Pop III stars as well as the distribution of the most massive Pop III stars based on an application of extreme-value statistics. Our calculations use the star formation rate density from a recent simulation to calibrate the star-formation efficiency from which the Pop III stellar abundances are derived. Our extreme-value modelling suggests that the most massive Pop III stars at redshifts $10 < z < 20$ are likely to be $\gtrsim 10^3 - 10^4 M_{\odot}$. Such extreme Pop III stars were sufficiently numerous to be the seeds of supermassive black holes at high redshifts and possibly source detectable gravitational waves. We conclude that the extreme-value formalism provides an effective way to constrain the stellar initial mass function.

Key words: stars: formation – stars: Population III – cosmology: dark ages, reionization, first stars.

1 INTRODUCTION

The hypothetical first generation of stars, so-called Population III (Pop III), have long been anticipated in the literature as massive, short-lived stars created in extremely metal-poor environments (Schwarzschild & Spitzer 1953; Bond 1981; Cayrel 1986; Carr 1994). Due to the lack of direct observational evidence, details of the physical properties of Pop III are not precisely known. Many studies suggest that Pop III stars were formed within minihaloes of typical mass $\sim 10^6 M_{\odot}$ between redshift $z \sim 20 - 30$ and have a mass range between $10 - 10^3 M_{\odot}$ (Haiman et al. 1996; Tegmark et al. 1997; Abel et al. 2002; Bromm et al. 2002; Yoshida et al. 2003; O’Shea & Norman 2007; Susa et al. 2014).

Interest in Pop III stars has grown recently due to current and upcoming experiments that could potentially detect Pop III stars. These include the *James Webb Space Telescope* (JWST; Gardner et al. (2006)), *Euclid* (Laureijs et al. 2011; Marchetti et al. 2017) and the *Roman Space Telescope* (RST; Spergel et al. (2015)). Confirmed observations of Pop III stars would solidify our understanding of stellar formation and evolution. However, the photometric signals from Pop III stars are expected to be very faint and would be extremely difficult to detect unless fortuitously enhanced by strong gravitational lensing (Zackrisson et al. 2012; Vikaeus et al. 2022).

Pop III stars are believed to end their lives in one of three channels: asymptotic giant branch stars, supernovae or black holes, depending on their masses. If the supernova progenitors have mass in the range $\sim 140 - 260 M_{\odot}$, they will ultimately form pair-instability supernovae

(PISNe) that are unique to Pop III star evolution (Moriya et al. 2019). If the Pop III progenitors are sufficiently massive, their collapse will also emit highly energetic gamma-ray bursts and after-glow components (Bromm & Loeb 2006; Kinugawa et al. 2019). Another possibility is that massive Pop III stars evolve with accretion rates of $0.1 - 1 M_{\odot} \text{ yr}^{-1}$ until gravitational instability triggers their collapse to black holes (Latif et al. 2013; Inayoshi et al. 2014; Umeda et al. 2016; Becerra et al. 2018; Haemmerlé et al. 2018).

Given the potential of Pop III stars to give rise to early massive black holes, Pop III stars may help us understand a longstanding conundrum in astrophysics: the origin of quasars at very high redshift $z \gtrsim 6$ (Fan et al. 2001; Willott et al. 2010; Mortlock et al. 2011; Matsuoka et al. 2019; Onoue et al. 2019; Das et al. 2021). Such high-redshift quasars are associated with supermassive black holes (SMBHs) with $M \gtrsim 10^9 M_{\odot}$ (Volonteri 2010; Inayoshi et al. 2020), which in turn could be seeded by Pop III stars with mass $M \sim 10^3 - 10^5 M_{\odot}$ that formed at redshift $z \gtrsim 10$. Such massive Pop III stars (which we call *extreme Pop III stars*) are certainly rare since most Pop III stars are expected to have mass $M \lesssim 10^2 M_{\odot}$ and are difficult to grow into SMBHs via accretion processes and mergers (Haiman & Loeb 2001; Haiman 2004; Volonteri 2010).

However there are many uncertainties in the formation channels of Pop III stars, and they may cover a wide mass range (Klessen & Glover 2023). In rare cases, the most massive objects form by direct collapse and such extreme Pop III stars are subject to general relativistic instabilities and can generate potentially detectable supernovae for precursors in a mass range around $3 \times 10^4 M_{\odot}$ (Nagele et al. 2022). Hence in our ensuing discussion, rather than attack the uncertain physics of Pop III star formation, we will use a novel statistical

★ E-mail: teeraparbc@nu.ac.th

approach to study the rarity of the most massive Population III stellar objects based on empirical constraints.

To summarise the importance of studying extreme Pop III stars:

(i) From an observational point of view, the first Pop III stars to be directly detected are likely to be amongst the most massive ones. The discovery of such objects will help us understand structure formation in the early universe and physics of the reionization epoch.

(ii) Extreme Pop III stars can explain the origin of SMBHs at high redshifts. If observed, follow-up observations will give us a better understanding of the environment and the conditions for SMBH formation.

In this work, we will demonstrate a formalism to calculate the mass distribution of the most massive Pop III stars based on extreme-value statistics. Our technique involves a novel calculation of *star formation rate density* (hereafter SFRD) which we discuss below.

There is no precise, universally agreed definition of Pop III stars. However, most literature defines Pop III stars based on criteria in metallicity. For instance, [Bond \(1981\)](#) defines Pop III stars as having $[\text{Fe}/\text{H}] < -3$ while [Komiya et al. \(2015\)](#) found that the metallicity of Pop III stars could span a wide range between $-8 \lesssim [\text{Fe}/\text{H}] \lesssim -2$ depending on the merging history of the host halos. Other authors use $Z < 10^{-3} - 10^{-5} Z_{\odot}$ where Z is the metal fraction ([Bromm et al. 2001](#); [Schneider et al. 2002](#); [Jaacks et al. 2018](#)). In our work, we shall define a generation of Pop III stars as a class of collapsed stellar objects with low metallicity forming when the host halo met the conditions described in section 3.

The organization of this article is as follows; In section 2 we give an introduction to the stellar initial mass function (IMF) which is used to calculate the abundance of Pop III stars. In section 3, we develop a theoretical formalism to calculate the star formation rate density (SFRD) of Pop III stars, matching our calculations to a simulation result. In section 4, we give an introduction to extreme-value statistics and, in particular, the Generalised Extreme Value approach. Our main results are given in section 5 and further implications are discussed in section 6.

2 THE STELLAR INITIAL MASS FUNCTION

The stellar initial mass function (hereafter IMF) is an important tool in the modelling of stellar abundances. The IMF expresses the number of stars (of a certain type at a fixed time) as a function of their mass. The IMF was first empirically proposed by [Salpeter \(1955\)](#) in the power-law form $\Phi(M) \equiv dN/d\log M \propto M^{-\Gamma}$, where N is the number of stars with mass between $\log M$ and $\log M + d\log M$. Γ is called the slope. The IMF $\Phi(M)$ describes the stellar mass distribution after their formation. In this work, we will study two IMFs for Pop III stars. First, the log-normal IMF

$$\frac{dN}{d\log M} \propto \exp\left(-\left(\frac{\log M - \log M_{\text{char}}}{\sqrt{2}\sigma}\right)^2\right), \quad (1)$$

where M_{char} is the characteristic mass of Pop III stars, and σ is the spread of the mass around M_{char} . The log-normal IMF was introduced in the pioneering work of [Miller & Scalo \(1979\)](#) who found the form to be a good fit to observation assuming simple models of star birthrates. Our second IMF model is the [Chabrier \(2003\)](#) IMF

$$\frac{dN}{d\log M} \propto M^{1-\alpha} \exp\left[-\left(\frac{M_{\text{char}}}{M}\right)^{\beta}\right], \quad (2)$$

with parameters α , β and M_{char} . This IMF has an interesting flexibility in that it resembles the log-normal IMF for small M and approaches

the power-law form $M^{1-\alpha}$ for large M (or when $\beta = 0$). An IMF comprising a log-normal body and a power-law tail is expected in a broad class of star-formation scenarios ([Basu & Jones 2004](#)). We note that the extreme-value framework that we will present is not limited to these IMFs.

The normalisation of the IMF is usually left unspecified in previous work on stellar population. Some authors treat Φ as a probability distribution (so that $\int d\log M \Phi = 1$), and normalise the number count N instead. Alternatively, one can also normalise the IMF using the total stellar mass, meaning that $M_{*}^{\text{total}} = \int_0^{\infty} d\log M M \Phi(M)$. Both normalisation methods depend on the measurement of either the stellar number counts or the total stellar mass for all possible masses of Pop III stars. Since direct observational constraints of Pop III stars are not yet feasible with current technologies, IMF normalisation with these methods are unreliable at best.

In this work, we propose another method of normalising the IMF using SFRD for which we have data from simulations ([Gessey-Jones et al. 2022](#)) (hereafter GJ22) which applied the star formation model from [Magg et al. \(2022\)](#). The normalised IMF is necessary for calculating the distribution of the most massive Pop III stars using extreme-value statistics. We discuss the normalisation method in the next section.

3 POP III STAR FORMATION RATE DENSITY - A NEW APPROACH

We shall develop a methodology to calculate the star formation rate density of Pop III stars based on the modelling of dark matter haloes ([Press & Schechter 1974](#)) and their cooling temperatures and time-scales ([Tegmark et al. 1997](#)). In our methodology, we propose that the total density of Pop III stars at redshift z is given by

$$\rho_{*,\text{III}}(z) = f_{*,\text{III}} \frac{\Omega_b}{\Omega_m} \int_{M_{\text{crit}}(z)}^{\infty} dM M \frac{dn}{dM}(M, z), \quad (3)$$

where $f_{*,\text{III}}$ is the Pop III star formation efficiency parameter, dn/dM is the halo mass function, and $n(M, z)$ is the number density of halo mass M at redshift z . Ω_b and Ω_m are respectively the baryonic and total matter density parameters at the present epoch.

$M_{\text{crit}}(z)$ is the critical minimum cooling mass of the host halo, given by ([Blanchard et al. 1992](#); [Tegmark et al. 1997](#)):

$$M_{\text{crit}}(z) = 1.0 \times 10^6 M_{\odot} \left(\frac{T_{\text{crit}}}{10^3 \text{ K}}\right)^{3/2} \left(\frac{1+z}{10}\right)^{-3/2}. \quad (4)$$

Haloes with mass below $M_{\text{crit}}(z)$ cannot efficiently dissipate their kinetic energy and become self-gravitating within a Hubble time. Our assumption is that once M exceeds M_{crit} , star formation will become effective. The value $T_{\text{crit}} = 2,200 \text{ K}$ (from considering molecular hydrogen cooling at redshift $z \sim 10$) will be used ([Hummel et al. 2012](#); [Magg et al. 2022](#)).

We further assume that $f_{*,\text{III}}$ is constant during the epoch where the stellar formation is dominated by Pop III stars (the effect of time-dependent $f_{*,\text{III}}$ will be discussed later in section 6). The redshift dependence of $\rho_{*,\text{III}}(z)$ therefore only comes from $M_{\text{crit}}(z)$ and $dn/dM(M, z)$.

The halo mass function, dn/dM , is defined as the redshift-dependent distribution of the number density of collapsed dark matter haloes per unit mass interval dM . It is convenient to express the mass function as

$$\frac{dn}{dM} = \frac{\rho_c}{M} \frac{d \ln \sigma^{-1}}{dM} f(\sigma), \quad (5)$$

where ρ_c is the critical density and $\sigma(M, z)$ is the variance of the

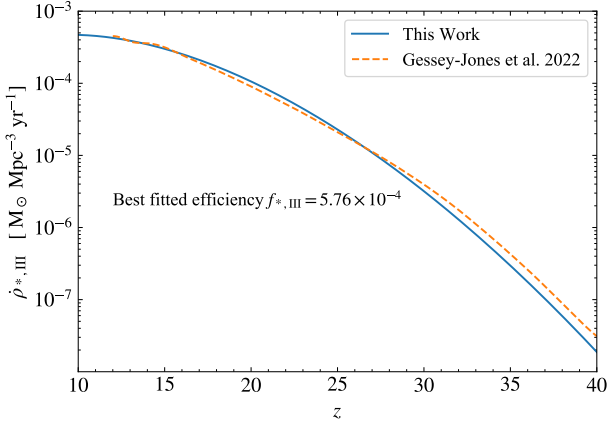


Figure 1. Comparison of the Pop III SFRD. We compare our Pop III SFRD (solid) to the simulation by Gessey-Jones et al. (2022) (dashed) and find the best-fitting Pop III star formation efficiency $f_{*,\text{III}} = 5.76 \times 10^{-4}$. The fiducial cosmology is based on Planck 2018 P1ik best-fitting parameters.

linear mass density field of mass M at redshift z . The multiplicity function $f(\sigma)$ (also known as the *mass fraction* (Jenkins et al. 2001)) is defined as the fraction of mass in collapsed haloes per unit interval in $\ln \sigma^{-1}$. The original Press-Schechter mass fraction, based on spherical collapse, is

$$f_{\text{PS}}(\sigma) = \sqrt{\frac{2}{\pi}} \frac{\delta_c}{\sigma} \exp\left[-\frac{\delta_c^2}{2\sigma^2}\right]. \quad (6)$$

The Press-Schechter mass fraction tends to underpredict the number of high-mass haloes and overpredict the number of low-mass haloes in the present epoch. It is also notably inaccurate at high redshifts (Lukić et al. 2007). Here, we will use the Sheth-Tormen mass function based on ellipsoidal collapse (Sheth & Tormen 1999). Its mass fraction is

$$f_{\text{ST}}(\sigma) = A \sqrt{\frac{2a}{\pi}} \frac{\delta_c}{\sigma} \exp\left(\frac{-a\delta_c^2}{2\sigma^2}\right) \left[1 + \left(\frac{\sigma^2}{a\delta_c^2}\right)^p\right], \quad (7)$$

with $A = 0.3222$, $a = 0.707$, $\delta_c = 1.686$, $p = 0.3$. This model gives a good fit to halo abundances in numerical simulations over a wide range of masses and redshifts (Lukić et al. 2007). Other mass functions have been discussed in the literature, including those by Jenkins et al. (2001), Barkana & Loeb (2004), Warren et al. (2006), Reed et al. (2007), Crocce et al. (2010) and Bhattacharya et al. (2011), with small deviations from the Sheth-Tormen mass function.

We make a simple observation that taking the time derivative of $\rho_{*,\text{III}}$ (equation (3)) gives the SFRD:

$$\dot{\rho}_{*,\text{III}}(z) = f_{*,\text{III}} \frac{\Omega_b}{\Omega_m} \left(\int_{M_{\text{crit}}(z)}^{\infty} dM M \frac{d\dot{n}}{dM} - \dot{M}_{\text{crit}} M \frac{dn}{dM} \right), \quad (8)$$

where a dot denotes time derivative. The first term on the right involves the time derivative of the mass function in equation (5). The second term depends on the time derivative of the critical mass in equation (4).

Our fiducial cosmology is based on Planck 2018 P1ik best-fitting parameters (Planck Collaboration et al. 2020). We compare our calculation with a semi-analytic simulation of GJ22 between $z = 12-40$ as shown in Fig. 1. We obtain the best-fitting value $f_{*,\text{III}} \approx 5.76 \times 10^{-4}$, which will be important in the extreme-value modelling in the next section.

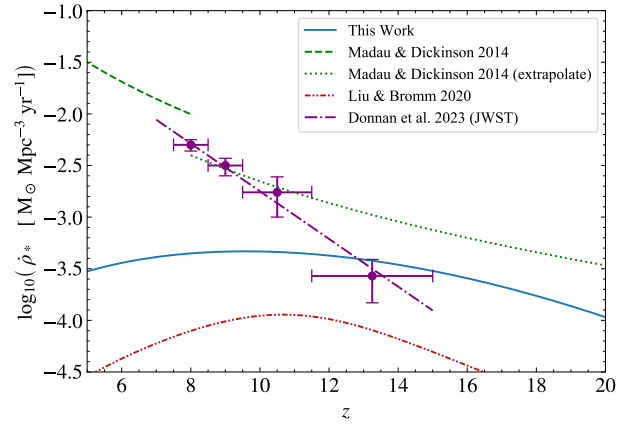


Figure 2. A comparison of SFRD from various models (listed in Table. 1) with observation from deep JWST (Donnan et al. 2023) (dashdotted). The model of Pop I + II from Madau & Dickinson (2014) (dashed) and its extrapolation with correction factor (dotted) are also shown for comparison (see description in section 6.1).

It is useful to obtain a fitting function of the SFRD. A particular template was suggested by Madau & Dickinson (2014) (hereafter MD14):

$$\frac{\dot{\rho}_{*}(z)}{\text{M}_{\odot}\text{yr}^{-1}\text{Mpc}^{-3}} = \frac{a(1+z)^b}{1 + [(1+z)/c]^d}, \quad (9)$$

where a, b, c and d are parameters in the fitting function. MD14 proposed this fitting function for Pop I and Pop II SFRD within $z \sim 0-8$. We have also calculated the parameters for the fitting function and listed them in Table 1 for our best-fitting $f_{*,\text{III}}$. The table also compares the values of the fitting parameters and the redshift range of validity from previous authors alongside ours. These models are plotted in Fig. 2, alongside the observational data from Donnan et al. (2023) (hereafter D23).

The data are from the *James Webb Space Telescope* and comprise the SFRD from all stellar populations in four redshift bins with mean redshifts $z = 8.0, 9.0, 10.5$ and 13.25 . Since the *JWST* data include contributions from Pop I and Pop II stars, it is not surprising that our estimate of the Pop III SFRD is below the data in the first three bins where Pop I and Pop II contributions to the SFRD are dominant. However, our Pop III SFRD agrees with the last bin at mean redshift $z = 13.25$ where the SFRD contribution is dominated by Pop III stars.

We can now use our SFRD calculation to normalise the IMF by equating equation (8) to the total number of stellar mass per unit time as determined by the stellar IMF $\Phi(M)$

$$\dot{\rho}_{*,\text{III}} = A(z) \int_0^{\infty} d \log M M \Phi(M), \quad (10)$$

where $A(z)$ is a redshift-dependent factor that normalises the first moment of the IMF per unit volume per unit time.

Once $A(z)$ is obtained, the IMF is normalised, and we can write down the number density of Pop III stars above mass M at redshift z (denoted $n(> M, z)$) as

$$n(> M, z) = A(z) \frac{dt}{dz} \int_M^{\infty} d \log M' \Phi(M'). \quad (11)$$

We will use this expression to calculate the mass of extreme Pop III stars.

Table 1. Fitting parameters for the SFRD using the functional form (9). The values of the parameters a , b , c and d for SFRD are listed alongside the redshift range and stellar types for which they are valid.

Reference	Redshift range	Type	Fitting parameters			
			a $M_{\odot} \text{ Mpc}^{-3} \text{ yr}^{-1}$	b	c	d
This work	6 – 20	Pop III	250.16	-4.744	14.74	-5.60
Madau & Dickinson (2014)	0 – 8	Pop I & II	0.015	2.7	2.9	5.6
Liu & Bromm (2020)	4 – 24	Pop III	765.7	-5.92	12.83	-8.55

4 EXTREME-VALUE STATISTICS

Our tool for quantifying the abundances of the most massive Pop III stars is extreme-value statistics. In particular, we will appeal to the generalised extreme-value (GEV) formalism - also known as the block maxima method. The quantity of interest is the probability distribution of block maxima, where a block is a population sample within a fixed volume. After dividing the data into N non-overlapping blocks, we collect the maximum value from each block. Under generic assumptions, the large- N limit (after a certain scaling) is one of three types: the Gumbel, Fréchet or Weibull distribution. This result is the celebrated Fisher-Tippett-Gnedenko theorem (analogous to the Central Limit theorem), which plays a key role in many real-world applications of extreme-value statistics. For an introduction to the GEV approach in extreme-value statistics, see de Haan & Ferreira (2006); Gomes & Guillou (2015).

The GEV approach has previously been used to quantify the abundances of the most massive galaxy clusters (Davis et al. 2011; Waizmann et al. 2012; Chongchitnan & Silk 2012) and primordial black holes (Kuhnel & Schwarz 2021). We believe this work is the first time the GEV formalism has been applied to Pop III stars.

Starting with the number density $n(> M, z)$ in equation (11), we can calculate the number density of Pop III stars of mass exceeding M in the entire redshift range $z \in [z_0, z_1]$ as

$$n(> M) = \int_{z_0}^{z_1} dz n(> M, z). \quad (12)$$

Now consider the probability that a region of volume V contains Pop III stars of mass not exceeding M . In other words, we are interested in the probability that no Pop III stars of mass $> M$ are found in the volume V . In the large volume limit, this probability can be described by the cumulative distribution function (cdf) of the Poisson form (White 1979; Davis et al. 2011)

$$P_0(M) = \exp(-n(> M)V). \quad (13)$$

By differentiating this cdf with respect to M , we obtain the pdf of the maximum mass Pop III stars within volume V .

In the limit that the Fisher-Tippett-Gnedenko theorem applies, we can equate the cdf (13) with the GEV distribution

$$G(M) = \begin{cases} \exp\left(-(1 + \gamma y)^{-1/\gamma}\right) & (\gamma \neq 0), \\ \exp(-e^{-y}) & (\gamma = 0), \end{cases} \quad (14)$$

where $y := (\log_{10} M - \alpha)/\beta$ is the scaled logarithmic mass. The parameter γ determines which of the 3 extremal types the block maxima converges to. The Gumbel, Fréchet and Weibull distributions correspond to $\gamma = 0$, $\gamma > 0$ and $\gamma < 0$ respectively.

The parameter γ as well as the scaling constants α and β can be determined as follows. By Taylor expanding the cdf $P_0(M)$ and the GEV $G(M)$ around the peak M_{peak} of the pdf to cubic order, we equate

terms and find that α, β, γ are given in terms of the redshift-averaged number density $n(> M)$ as:

$$\gamma = n(> M_{\text{peak}})V - 1 \quad \beta = \frac{(1 + \gamma)^{1+\gamma}}{\left. \frac{dn}{dM} \right|_{M_{\text{peak}}}} M_{\text{peak}} V \ln 10$$

$$\alpha = \log_{10} M_{\text{peak}} - \frac{\beta}{\gamma} \left((1 + \gamma)^{-\gamma} - 1 \right). \quad (15)$$

These values allow us to characterise the extreme-value distribution of Pop III stars. In particular, α corresponds roughly to the peak mass $\log_{10} M_{\text{peak}}$, and $\gamma + 1$ is the number count of stars with mass above M_{peak} . These GEV parameters are important in the modelling of extreme objects because they allow us to venture into domains of small probabilities which would have been numerically prohibitive to calculate otherwise.

5 EXTREME POP III STARS

Two plots of the pdfs for the maximum-mass Pop III stars in the redshift range $z \in [10, 20]$ obtained via extreme-value modelling are shown in Fig. 3 and Fig. 4. In Fig. 3 we use the log-normal IMF (eq. 1) with parameters $M_{\text{char}} = 1 M_{\odot}$ and $\sigma = 1$, whilst Fig. 4 uses the Chabrier model (eq. 2) with $\alpha = 5, \beta = 1$ and $M_{\text{char}} = 1 M_{\odot}$. In both models, we assume full-sky observation ($f_{\text{sky}} = 1$). The four curves in each plot correspond to varying values of $f_{*,\text{III}}$, with the value 5.76×10^{-4} being the best-fitting value obtained from the SFRD methodology described in section 3. For these parameter choices, the pdfs peak at around $\sim 10^3 - 10^4 M_{\odot}$ for the best-fit $f_{*,\text{III}}$. The possibility of such large values of extreme-mass Pop III stars has been hypothesized previously (Haemmerlé et al. 2018).

Next, we found that the value of the GEV parameter γ (which determines the extremal type) are typically small ($|\gamma| \lesssim 0.05$) with the possibility of both positive and negative values. Essentially the pdfs are well described by the Gumbel distribution ($\gamma = 0$). This is similar to the conclusion in Davis et al. (2011) who studied the GEV fit for massive clusters. This conclusion is also consistent with the theoretical result that extreme values from the log-normal distribution follow the Gumbel distribution in the limit that the Fisher-Tippett theorem holds. See Embrechts et al. (1997) for details.

In addition, we note that in both models increasing $f_{*,\text{III}}$ by an order of magnitude shifts the pdfs towards higher extreme masses by roughly a factor of 2. Overall the extreme-mass predictions are quite robust against changes in $f_{*,\text{III}}$.

However, the extreme-mass predictions are much more sensitive to changes in some of the parameters of the IMF (and indeed, the form of the IMF itself). We argue that the extreme-value formalism can be used to constrain the model parameters by considering the prediction of the extreme masses of Pop III stars. This is demonstrated in Fig. 5

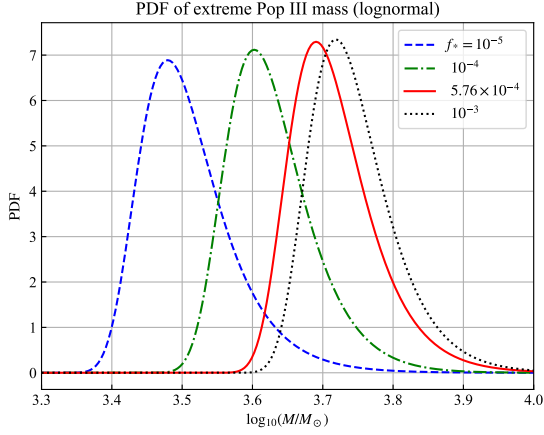


Figure 3. The probability density functions for the extreme-mass Pop III stars for $10 < z < 20$, assuming the log-normal IMF (eq. 1) with $\sigma^2 = 1$ and $M_{\text{char}} = 1 M_{\odot}$. The 4 curves correspond to 4 values of $f_{*,\text{III}}$. The curve corresponding to $f_{*,\text{III}} = 5.76 \times 10^{-4}$ (solid red line) uses the best-fitting star-formation efficiency obtained from fitting to the simulation of GJ22.

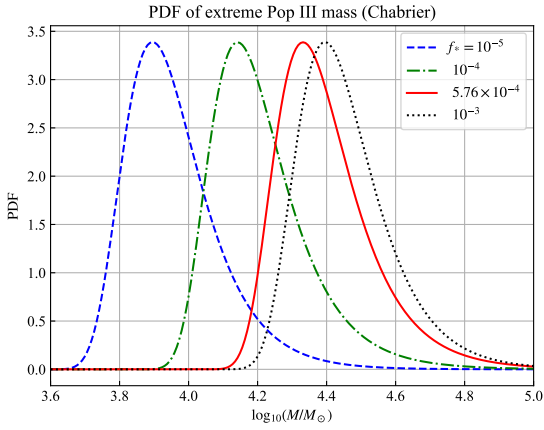


Figure 4. Same as Fig. 3 but for the Chabrier IMF (eq. 2) with $\alpha = 5$, $\beta = 1$ and $M_{\text{char}} = 1 M_{\odot}$.

and Fig. 6 in which we vary the IMF parameters and note the peak of the extreme-value pdf.

In Fig. 5, we vary M_{char} against σ^2 in the log-normal model. In 6, we vary M_{char} against α in the Chabrier model (fixing $\beta = 1$ - the extreme peaks are insensitive to changes in β). In both contour plots, we use the best-fit value of $f_{*,\text{III}} = 5.76 \times 10^{-4}$. We see that a wide range of extreme Pop III masses $\gtrsim 10^3 - 10^4 M_{\odot}$ are possible. Portions of such IMF parameter space can be effectively ruled out with future observations of massive Pop III stars.

We observe that extreme masses of order $\sim 10^3 - 10^4 M_{\odot}$ arise naturally out of the EVS formalism. Calculating the number density $n(> M)$ reveals that Pop III stars of mass $\gtrsim 10^3 M_{\odot}$ can in fact form in significant abundances in a wide range of parameter space. For instance, in the log-normal model with $M_{\text{char}} = 1 M_{\odot}$, taking $\sigma \gtrsim 0.7$ yields $n(> 10^3 M_{\odot})$ exceeding 10^{-9}Mpc^{-3} . This translates to a number count of $N \gtrsim 10^3$ objects in $10 < z < 20$. Such an abundance of massive Pop III stars is ideal for seeding massive black holes at high redshifts, in addition to black holes of primordial origin (Chongchitnan et al. 2021).

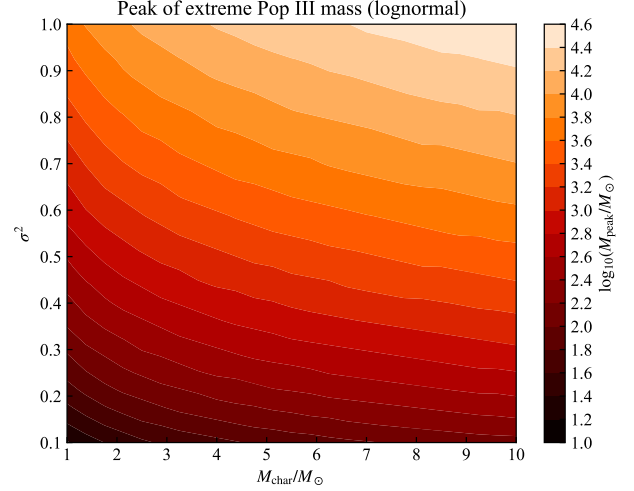


Figure 5. Heat map showing M_{peak} , the peak of the extreme-value PDF (in $z \in [10, 20]$) as a function of the log-normal IMF (eq. 1) with parameters σ^2 and M_{char} , whilst fixing $f_{*,\text{III}} = 5.76 \times 10^{-4}$.

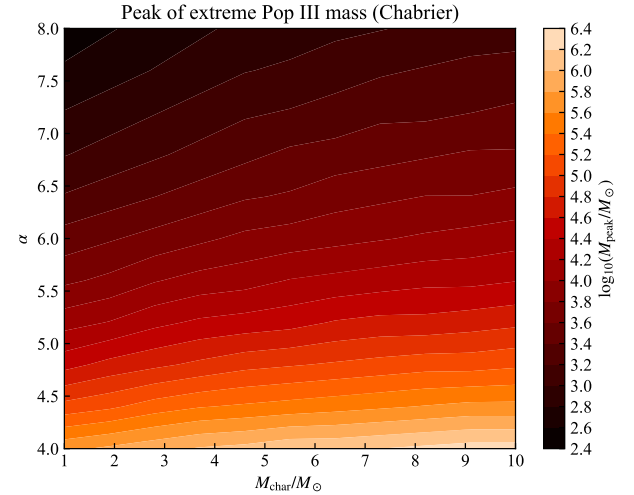


Figure 6. Heat map showing M_{peak} , the peak of the extreme-value PDF (in $z \in [10, 20]$) as a function of the Chabrier IMF (eq. 2) with parameters α and M_{char} , whilst fixing $\beta = 1$ and $f_{*,\text{III}} = 5.76 \times 10^{-4}$.

6 CONCLUSION AND DISCUSSION

6.1 Pop III SFRD

We have presented a novel methodology for calculating the Pop III SFRD and star formation efficiency $f_{*,\text{III}}$ (equation (8)). We assumed that $f_{*,\text{III}}$ is constant which is a plausible assumption since the metallicity of Pop III stars varies slowly. Jaacks et al. (2018) has shown that the mean metallicity Z rises smoothly from $z \approx 25$ reaching $Z_{\text{crit}} = 10^{-4} Z_{\odot}$ at $z \approx 7$ where Z_{crit} is the transition metallicity for the Pop III to Pop II stars. Thus, we would expect $f_{*,\text{III}}$ to also increase slowly with time. To implement this, we could add an extra term involving $\dot{f}_{*,\text{III}}$ in equation (8), where $\dot{f}_{*,\text{III}}$ is small. Even with a varying efficiency, we expect the effect on the SFRD to be small.

The assumptions made in our methodology are sufficient for a good fit to be achieved in comparison with the simulation from GJ22 in Fig. 1 and observational data from deep JWST (D23) in Fig. 2.

We also gave a fitting function for our SFRD in equation (9), shown

in Fig. 2 along with those of previous authors, including MD14 and Liu & Bromm (2020). It is interesting to note that MD14 proposed this fitting function for Pop I and Pop II stars, and therefore the function has a limited validity range $z = 0 - 8$. A direct extrapolation of MD14 to higher redshifts overestimates the SFRD; however, as anticipated by Shapley et al. (2023), the conversion factor between $H\alpha$ luminosity and SFRD should be lower by a factor of ~ 2.5 . We apply the correction factor of 2.5 to MD14 extrapolation and obtained an improved consistency with the JWST data.

We provide our fitting function for the Pop III SFRD in Table 1. It only matches our Pop III SFRD well within $z = 6 - 20$, beyond which the functional form fails to capture the rapid decrease in the SFRD at higher redshifts. Nevertheless, our fitting function should be useful for calculations involving the total SFRD.

In comparison, D23 has also provided a simple fitting function for their data (in Fig. 2) with limited validity range as

$$\log_{10} \dot{\rho}_* = (-0.231 \pm 0.037) \times z - (0.43 \pm 0.3), \quad (16)$$

where $\dot{\rho}_*$ is the SFRD in unit of $M_{\odot} \text{ Mpc}^{-3} \text{ yr}^{-1}$. The validity range of the fitting function in equation (16) is only from $z \sim 7 - 13$. We recommend using the fitting function in equation (16) within its validity range together with our fitting function at higher redshifts for the total SFRD (See Table 1).

6.2 Extreme Pop III stars

We applied the SFRD methodology to the calculation of the probability distribution of the most massive Pop III stars expected in the redshift range 10 to 20. Adoption of a functional form of the stellar IMF allowed the IMF to be normalised, and the number density of Pop III stars can then be calculated. The extreme-value pdf were then derived as shown in Fig. 3 and 4. We demonstrated that for a wide range of parameter values in the log-normal and Chabrier IMF, extreme Pop III stars of mass $\sim 10^3 - 10^4 M_{\odot}$ arose naturally, and even higher masses are achievable. We conclude that extreme-value statistics can help effectively constrain the IMF of Pop III stars. In addition, Extreme Pop III stars are a viable channel for producing high-redshift quasars and massive black-holes whose gravitational-wave signals may be detectable by *LIGO*¹ or the next generation of gravitational wave observatories such as the Einstein Telescope² and *LISA*³. In short, our predicted extreme Pop III stars are plausible candidates for seeding SMBH at high redshifts. They form $10^3 - 10^4 M_{\odot}$ BH at early epochs, allow the required numbers of e-folds of growth by Eddington-limited accretion, and are rare but still sufficiently numerous to solve the seeding problem for high-redshift quasars.

ACKNOWLEDGEMENTS

We would like to thank Thomas Gessey-Jones for his kind provision of the data and useful suggestions. Without the data, our work would be far from complete. We also thank Suraphong Yuma and Tirawut Worrakitpoonpon for their suggestions. “This work was supported by Naresuan University (NU), and the National Science, Research and Innovation Fund (NSRF). Grant NO. R2566B091.

¹ <https://www.ligo.org>

² <https://www.et-gw.eu>

³ <https://lisa.nasa.gov>

DATA AVAILABILITY

The data underlying this article will be shared on reasonable request to the corresponding author.

REFERENCES

- Abel T., Bryan G. L., Norman M. L., 2002, *Science*, 295, 93
 Barkana R., Loeb A., 2004, *ApJ*, 609, 474
 Basu S., Jones C. E., 2004, *MNRAS*, 347, L47
 Becerra F., Marinacci F., Bromm V., Hernquist L. E., 2018, *MNRAS*, 480, 5029
 Bhattacharya S., Heitmann K., White M., Lukić Z., Wagner C., Habib S., 2011, *ApJ*, 732, 122
 Blanchard A., Valls-Gabaud D., Mamon G. A., 1992, *A&A*, 264, 365
 Bond H. E., 1981, *ApJ*, 248, 606
 Bromm V., Loeb A., 2006, *ApJ*, 642, 382
 Bromm V., Ferrara A., Coppi P. S., Larson R. B., 2001, *MNRAS*, 328, 969
 Bromm V., Coppi P. S., Larson R. B., 2002, *ApJ*, 564, 23
 Carr B., 1994, *ARA&A*, 32, 531
 Cayrel R., 1986, *A&A*, 168, 81
 Chabrier G., 2003, *PASP*, 115, 763
 Chongchitnan S., Silk J., 2012, *Phys. Rev. D*, 85, 063508
 Chongchitnan S., Chantavat T., Zunder J., 2021, *Astronomische Nachrichten*, 342, 648
 Crocce M., Fosalba P., Castander F. J., Gaztañaga E., 2010, *MNRAS*, 403, 1353
 Das A., Schleicher D. R. G., Basu S., Boekholt T. C. N., 2021, *MNRAS*, 505, 2186
 Davis O., Devriendt J., Colombi S., Silk J., Pichon C., 2011, *MNRAS*, 413, 2087
 Donnan C. T., et al., 2023, *MNRAS*, 518, 6011
 Embrechts P., Klüppelberg C., Mikosch T., 1997, *Modelling extremal events: for insurance and finance*. Springer, Heidelberg
 Fan X., et al., 2001, *AJ*, 122, 2833
 Gardner J. P., et al., 2006, *Space Sci. Rev.*, 123, 485
 Gessey-Jones T., et al., 2022, *MNRAS*, 516, 841
 Gomes M. I., Guillou A., 2015, *International Statistical Review*, 83, 263
 Haemmerlé L., Woods T. E., Klessen R. S., Heger A., Whalen D. J., 2018, *MNRAS*, 474, 2757
 Haiman Z., 2004, *ApJ*, 613, 36
 Haiman Z., Loeb A., 2001, *ApJ*, 552, 459
 Haiman Z., Thoul A. A., Loeb A., 1996, *ApJ*, 464, 523
 Hummel J. A., Pawlik A. H., Milosavljević M., Bromm V., 2012, *ApJ*, 755, 72
 Inayoshi K., Omukai K., Tasker E., 2014, *MNRAS*, 445, L109
 Inayoshi K., Visbal E., Haiman Z., 2020, *ARA&A*, 58, 27
 Jaacks J., Thompson R., Finkelstein S. L., Bromm V., 2018, *MNRAS*, 475, 4396
 Jenkins A., Frenk C. S., White S. D. M., Colberg J. M., Cole S., Evrard A. E., Couchman H. M. P., Yoshida N., 2001, *MNRAS*, 321, 372
 Kinugawa T., Harikane Y., Asano K., 2019, *ApJ*, 878, 128
 Klessen R. S., Glover S. C. O., 2023, *arXiv e-prints*, p. arXiv:2303.12500
 Komiya Y., Suda T., Fujimoto M. Y., 2015, *ApJ*, 808, L47
 Kuhnel F., Schwarz D. J., 2021, *arXiv e-prints*, p. arXiv:2101.10340
 Latif M. A., Schleicher D. R. G., Schmidt W., Niemeyer J., 2013, *MNRAS*, 433, 1607
 Laureijs R., et al., 2011, *arXiv e-prints*, p. arXiv:1110.3193
 Liu B., Bromm V., 2020, *MNRAS*, 497, 2839
 Lukić Z., Heitmann K., Habib S., Bashinsky S., Ricker P. M., 2007, *ApJ*, 671, 1160
 Madau P., Dickinson M., 2014, *ARA&A*, 52, 415
 Magg M., et al., 2022, *MNRAS*, 514, 4433
 Marchetti L., Serjeant S., Vaccari M., 2017, *MNRAS*, 470, 5007
 Matsuoka Y., et al., 2019, *ApJ*, 883, 183
 Miller G. E., Scalo J. M., 1979, *ApJS*, 41, 513

- Moriya T. J., Wong K. C., Koyama Y., Tanaka M., Oguri M., Hilbert S., Nomoto K., 2019, *PASJ*, **71**, 59
- Mortlock D. J., et al., 2011, *Nature*, **474**, 616
- Nagele C., Umeda H., Takahashi K., Yoshida T., Sumiyoshi K., 2022, *MNRAS*, **517**, 1584
- O’Shea B. W., Norman M. L., 2007, *ApJ*, **654**, 66
- Onoue M., et al., 2019, *ApJ*, **880**, 77
- Planck Collaboration et al., 2020, *A&A*, **641**, A6
- Press W. H., Schechter P., 1974, *ApJ*, **187**, 425
- Reed D. S., Bower R., Frenk C. S., Jenkins A., Theuns T., 2007, *MNRAS*, **374**, 2
- Salpeter E. E., 1955, *ApJ*, **121**, 161
- Schneider R., Ferrara A., Natarajan P., Omukai K., 2002, *ApJ*, **571**, 30
- Schwarzschild M., Spitzer L., 1953, *The Observatory*, **73**, 77
- Shapley A. E., Sanders R. L., Reddy N. A., Topping M. W., Brammer G. B., 2023, *arXiv e-prints*, p. arXiv:2301.03241
- Sheth R. K., Tormen G., 1999, *MNRAS*, **308**, 119
- Spergel D., et al., 2015, *arXiv e-prints*, p. arXiv:1503.03757
- Susa H., Hasegawa K., Tominaga N., 2014, *ApJ*, **792**, 32
- Tegmark M., Silk J., Rees M. J., Blanchard A., Abel T., Palla F., 1997, *ApJ*, **474**, 1
- Umeda H., Hosokawa T., Omukai K., Yoshida N., 2016, *ApJ*, **830**, L34
- Vikaeus A., Zackrisson E., Schaerer D., Visbal E., Fransson E., Malhotra S., Rhoads J., Sahlén M., 2022, *MNRAS*, **512**, 3030
- Volonteri M., 2010, *A&ARv*, **18**, 279
- Waizmann J. C., Etori S., Moscardini L., 2012, *MNRAS*, **420**, 1754
- Warren M. S., Abazajian K., Holz D. E., Teodoro L., 2006, *ApJ*, **646**, 881
- White S. D. M., 1979, *MNRAS*, **186**, 145
- Willott C. J., et al., 2010, *AJ*, **139**, 906
- Yoshida N., Abel T., Hernquist L., Sugiyama N., 2003, *ApJ*, **592**, 645
- Zackrisson E., et al., 2012, *MNRAS*, **427**, 2212
- de Haan L., Ferreira A., 2006, *Extreme Value Theory: an introduction*. Springer, New York

This paper has been typeset from a $\text{\TeX}/\text{\LaTeX}$ file prepared by the author.